JOURNAL OF MATERIALS SCIENCE **39** (2004) 5659– 5667

Thermal stability study on two aluminum alloys processed with equal channel angular pressing

M. CABIBBO*, E. EVANGELISTA, V. LATINI
INFM—Department of Mechanics, Polytechnic University of Marche, I-60131, Ancona, Italy
E-mail: marcello.cabibbo@unian.it

Equal channel angular pressing was used to produce sub-micrometer size grain structures in two aluminum alloys (commercially pure 1200 and Al-Mn-Si 3103). ECAP was conducted at room temperature following the process via "route C," which involves a 180° angular rotation between passes and strongly affects material microstructure by reversing the shear strain every second pass. This unique characteristic of route C induced limited build-up of new high-angle boundaries, at least for the first three passes. The equal channel angular pressing was extended to six passes for both alloys; three passes by route C throughout the die were sufficient to produce a very fine-structured material for both alloys. High-resolution electron back-scattered diffraction pattern analysis was carried out to measure boundary misorientation within the deformed structures. Measurements of subgrain and grain spacing revealed a more effective microstructure refining effect in the 3103 than the 1200 alloy. Thermal stability of the severely deformed materials was studied at temperatures of 130, 240, 330°C, corresponding to 0.2, 0.35, 0.5 of the melting temperature. The results showed considerable grain growth in both materials solely at temperatures from and above half of the melting one.

1. Introduction

It is well known that heavy deformations (i.e., by cold-rolling or drawing) can produce a refined microstructure also at low-temperatures [1–6]. In particular, nano-structured materials produced by severe plastic deformation (SPD) are ultrafine-grained structures of granular type having mainly high-angle grain boundaries [1–5]. Special methods are required to apply SPD to metallic materials: these are essentially severe torsion straining under high pressure, equal channel angular pressing (ECAP), high-energy ball milling, and sliding wear [1, 7]. However, by using the last two procedures residual porosity remains after material production and it is thus difficult to use these techniques to make large-scale bulk samples. As a consequence, greater attention has been addressed to the first two, novel, refining techniques. In particular, the ECAP process is capable of producing large, fully-dense samples having an ultrafine grain size in the sub-micrometer range [8, 9]. The ECAP process has its major advantage in maintaining the billet shape unchanged. Moreover, ECAP processed samples are free of any porosity; the process can thus be used to manufacture large bulk samples for a wide range of industrial applications. The process is currently applied to different materials ranging from Al to Cu, Mg, Ti and ferrous alloys [8–14].

In ECAP, the billet is pressed into the die channel several times, each time multiplying the equivalent strain to which it is subjected. Equation 1 illustrates the dependency of the equivalent strain as a function of angles Φ and Ψ characterizing the two intersecting channel of the die [2, 15–18]:

$$\varepsilon_N = \frac{N}{\sqrt{3}}\left[2\cot\left(\frac{\Phi}{2}+\frac{\Psi}{2}\right)+\Psi\mathrm{cosec}\left(\frac{\Phi}{2}+\frac{\Psi}{2}\right)\right] \quad (1)$$

where N is the number of passes. Samples can be repeatedly introduced into the top channel of the die in different ways, which the literature designates as "routes" [16]. The routes are physically distinguished by the shear directions introduced at each pass through the intersecting channels of the die. In particular, "route C" does not involve any change in the pressing direction [1]. Moreover, as a general rule, a considerable increase in yield stress, strength (by the refining effect on the microstructure) and ductility until the process reaches saturation occurs after N passes which usually range from 12 to 15 depending on the specific "route" and on the material [16, 19, 20].

To date, two different and complementary techniques have mainly been used in order to investigate the microstructure of materials subjected to ECAP. One consists of transmission electron microscopy (TEM) investigations combined with selected area electron diffraction (SAED) pattern [7, 9, 10, 15, 17, 20, 21], whilst the second is based on electron back-scattered

*Author to whom all correspondence should be addressed.

diffraction (EBSD) pattern performed with a high-resolution field emission gun scanning electron microscope (FEG-SEM) [3–6, 8, 10, 22]. By TEM inspections microstructure refinement (i.e., the transformation of subgrain into grain) can be qualitatively detected by means of the spread of the SAED spots, and it is particularly suitable for the study of subgrain structure and dislocation density evolution during the deformation. EBSD, especially when performed with a FEG-SEM, is generally used to measure shape, size and distribution of cells as small as ∼200 nm in width, and a single EBSD map may contain several thousand cells or subgrains. EBSD also provides detailed information on the orientation distribution of both subgrains and grains, which is time-consuming and difficult to obtain by means of TEM inspections. A current limitation of EBSD analysis is that it involves an angular resolution which can hardly approach ∼1.5–2°, and this means that very low-angle boundaries or cell walls are usually not detected [3, 4].

The present paper aims at illustrating the early results obtained with EBSD acquired using a FEG-SEM performed on ECAP processed 1200 and 3103 aluminum alloys using route C. The study was limited to the first six ECAP passes for both alloys. Thermal stability was studied in order to establish the effectiveness and stability of the microstructure grain refinement induced by ECAP.

2. Experimental details

The two aluminum alloys, 1200 and 3103, were produced by Hydro (Norway); prior to ECA pressing, they were homogenized at 340°C for 4 h, then air-cooled. Table I reports their chemical composition. The microstructure of the solution treated materials (not-deformed materials) had a mean grain size of ∼40 and ∼20 μm for the 1200 and the 3103 alloy, respectively.

All of the ECA pressings were conducted at room-temperature using a solid die fabricated from a block of SK3 tool steel (Fe-1.1%C) and endowed with two cylindrical channels intersecting at an angle $\Phi = 90^\circ$ and a curvature $\Psi = 20^\circ$. Based on Equation 1, this configuration allowed to introduce an equivalent strain of $\varepsilon \approx 1$ ($\varepsilon = 1.055$) at each pass. Samples and channels were coated with a spray lubricant containing MoS_2. The deformation route C was used, which involves a specimen rotation of 180° at each pass.

EBSD investigations were conducted by scanning a rectangular area of halfway cut samples in the pressing-transverse direction (PD-TD) plane. Samples for EBSD were prepared by polishing the surface up to 0.25 μm diamond paste followed by electro-chemical polishing in colloidal silica suspension; finally the surface was electro-polished with a 30% HNO_3 solution in methanol, working at $V = 12$ V, at a temperature of −30°C. A FEG-SEM equipped with EBSD was used for grain and subgrain spacing and orientation distribution measurements. Due to the limitations mentioned above, only boundaries with misorientation greater than 1.5–2° were recorded on the EBSD maps; free dislocations and any cells with boundaries with misorientation less than 2° thus remained unresolved. Subgrain and grain aspect ratio was measured by averaging the values of at least 4 sample regions in each sample using an image analyzer.

A reversed Leika light microscope (LM) was used to qualitatively estimate the microstructure refining process. All specimens' surfaces were anodized along the PD-TD plane using a 5% HBF_4 solution in methanol at a voltage $V = 20$ V, and current $i = 30$ mA at room-temperature. The PD-TD plane is depicted in Fig. 1.

For the thermal stability investigations, a conventional furnace was used; temperatures ranged from 130 to 330°C and exposure duration was 1 h. Microhardness tests were carried out using a Vickers diamond pyramid indenter; tests were conducted with a load of 100 g for 15 s; each data constitutes a statistical value based on over 11 independent measurements.

TABLE I Chemical composition of the 1200 and 3103 alloys (wt%)

	Mn	Mg	Si	Fe	Cu	Cr	Zn	Ti	Al
1200 alloy	0.008	0.006	0.008	0.008	0.002	0.002	0.006	0.002	Bal.
3103 alloy	0.50	0.45	0.55	0.60	0.30	0.20	0.35	0.10	Bal.

3. Results

Figs 2 and 3 show some representative LM micrographs of anodized surfaces of both ECA pressed materials; the EBSD map is also reported for the corresponding conditions. In the LM micrographs, the different gray contrasts correspond to different grain orientations; the corresponding EBSD maps reveal similar aspects and here all thick black lines indicate the location of high-angle boundaries (i.e., the boundaries having a relative misorientation greater than 15°).

Both LM and EBSD maps of the materials subjected to 1 pass show a microstructure decorated by elongated grains along the shear bands introduced during ECA pressing. In particular, the EBSD map clearly showed the grain interior structure to consist of many subgrains oriented mainly along the shear direction and forming an angle of ∼45° with respect to the pressing direction. At this stage, narrow, widely spaced intersecting bands began to shear the bands of elongated cells. This led either to offsets in the elongated cell bands which had been sheared, and to the formation of ledges along grain boundaries in grains where the shearing was particularly pronounced; according to F.J. Humphreys, these ledges can be referred to as micro-shear bands [23]. After 2 passes, the ECAP-processed materials showed a reconstitution trend of quasi-equiaxed grain structure due to the reversal of shear direction at each even pass. With a rotation of 180°, the billet simply deformed in one plane, basically involving shear strain reversion and this results in a redundant strain. The microstructure consisted of quasi-equiaxed grains with shape similar to the starting grain size (i.e., the ones of the non-deformed material); the corresponding EBSD map shows a grain interior decorated by diffuse subgrain boundaries (Fig. 3). Low-angle boundaries could be identified within the grains, and the material

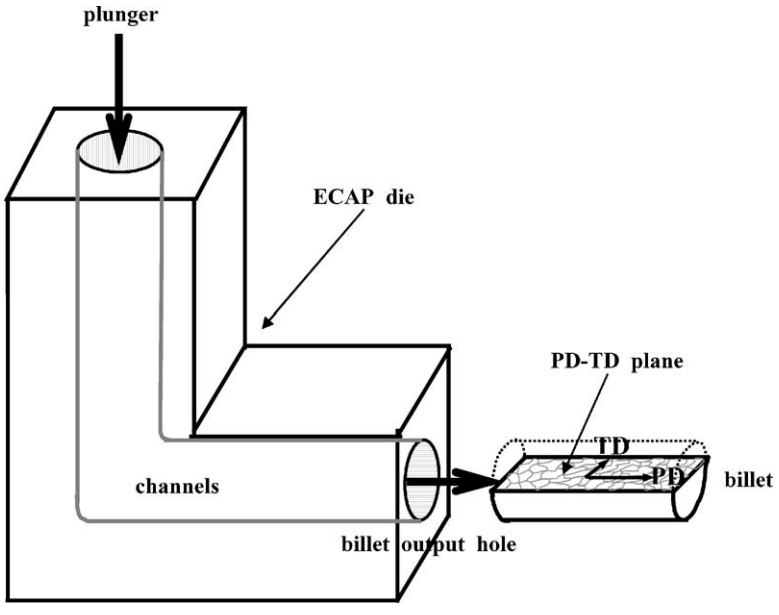

Figure 1 Scheme of the PD-TD plane.

contained large regions entirely consisting of subgrains within fine micrometric grains. The microstructure of the 1200 alloy differed from the one of the 3103 alloy in two major aspects. One was the clear and diffuse presence of white areas in the 3103 alloy's maps, prevalently located along the grain boundaries and this is mainly due to the second-phase particles, precipitated during the homogenization of 3103 alloy. The other aspect was the wider subgrain cell spacing in the 1200 alloy, suggesting a pinning phenomenon of fine (Mn, Fe)Al_6 second-phase precipitates, which inhibited subgrain cell growth in the 3103 alloy. After 3 passes, the microstructure of ECA pressed materials consisted again of elongated grains and was quite similar to the one observed after 1 pass except for a larger high-angle grain boundary (HAGB) volume fraction present in the microstructure of 3-ECAP passes materials. In the 1200 alloy, the 5th pass produced a very fine grain microstructure. Comparison between 1200 and 3103 ECA pressed alloys showed a more effective microstructure refining process in the latter alloy, in which a very fine microstructure was produced already after 3 passes. As a result, the microstructure of 3103 after 3 passes was quite similar to the one of 1200 subjected to 5 passes.

In Fig. 4 a plot of the subgrain and grain spacing, together with the HAGB fraction, as a function of the true stress (i.e., ECAP passes), for both 1200 and 3103 alloys, is shown. ECAP induced a consistent grain breaking-up process with increasing strain, which is responsible for the drastic increment of the very-fine grain fraction at the expense of the subgrains. These latter, continuously decreased in size, but also in volume fraction, creating new very fine HAB grains, thus the HAGB increase corresponded to the grain and subgrain spacing decrease. Yet, the refining process was more effective in the 3103 than 1200 alloy. The 3rd pass was sufficient to produce a very fine grain structure with a main grain size less than 2 μm for both alloys.

Static annealing tests showed that the ultrafine grain structure, produced by ECA pressing, was practically stable in both alloys for temperatures below 240°C (corresponding to 0.35 T_m). For temperatures of 0.35 T_m mean grain dimension started to increase, although their mean spacing remained sub-micrometric or less than 2–3 microns. However, the annealing tests demonstrated the failure of both the alloys to retain an ultrafine grain and subgrain size microstructure at the sub-micrometric range for temperatures above 240°C (0.35 T_m).

4. Discussion

4.1. EBSD analysis

High-angle grain boundary tended to increase in volume fraction at the expense of lower-angle boundaries, while subgrain mean misorientation appeared to remain practically stable with ECAP passes, and correspondingly, the number of passes induced a noticeable grain refinement. This suggested the ECAP refining process to be characterized by a subgrain misorientation increase from low-angle (about 4–5°) to high-angle (at least 15°) under the effect of the various passes without any significant appearance of medium-angle boundaries. Indeed, the deformed microstructure seems to be able to retain the imposed deformation without involving serious changes in subgrain misorientation. The microstructure breaking-up phenomenon, involved in route C, was documented by the decreasing of all the curves slopes reported in Fig. 4. In fact, grains and subgrains spacing decreasing trend with the ECAP passes showed a pause for every even passes in which the microstructure refining process was far away less effective respect to all the odd passes. This holds also for the HAGB fraction increasing trend, which correspondingly changed its slope at every even pass. Similarly, it was possible to detect this peculiar characteristic by means of the pause in the subgrain fraction decreasing with the ECAP passes. In the 1200 alloy, even passes induced a slight overall increase and odd passes a pause

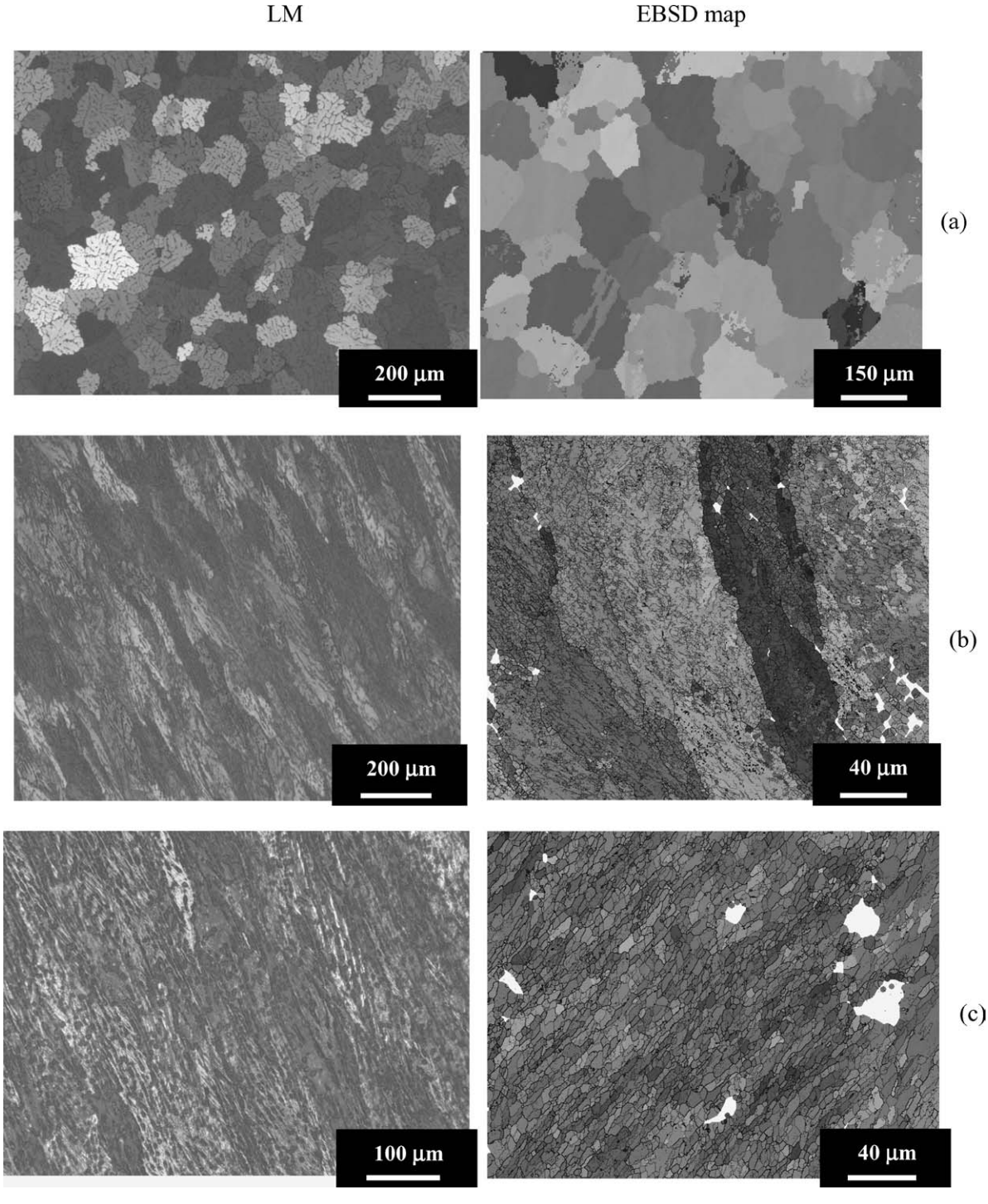

Figure 2 Representative LM micrographs and EBSD maps of the 1200 alloy for the not-deformed (a), after 1 pass (b), and 5 passes (c). In the EBSD maps, the thick black lines stand for grain boundaries.

in the high-angle trend. The 3103 alloy showed essentially consistent average angular grain misorientation over all ECAP passes; this difference may be attributed to the presence of fine dispersed Al_6Mn second-phase particles.

4.2. Thermal stability

The presence of a high volume fraction of high-angle boundaries in a material is an important prerequisite to achieve high tensile ductility. This is due to the flow process during the super-plastic deformation mainly generated by grain boundary sliding. Indeed, the microstructure of both severely deformed alloys is decorated by a large volume fraction of low-angle subgrain boundaries, resulting in overall heterogeneity. A strong presence of such low-angle subgrain boundaries has been showed to considerably limit the capability of the Al-alloy to achieve high tensile ductility [21]. The thermal stability study was thus performed to evaluate the tendency of high-angle grain boundaries to migrate and the low-angle subgrain boundaries tendency to transform into high-angle ones, or to disappear under the effect of the different ageing treatments.

Grain size evaluation of the two ECAP processed materials and heat treatment was performed according to

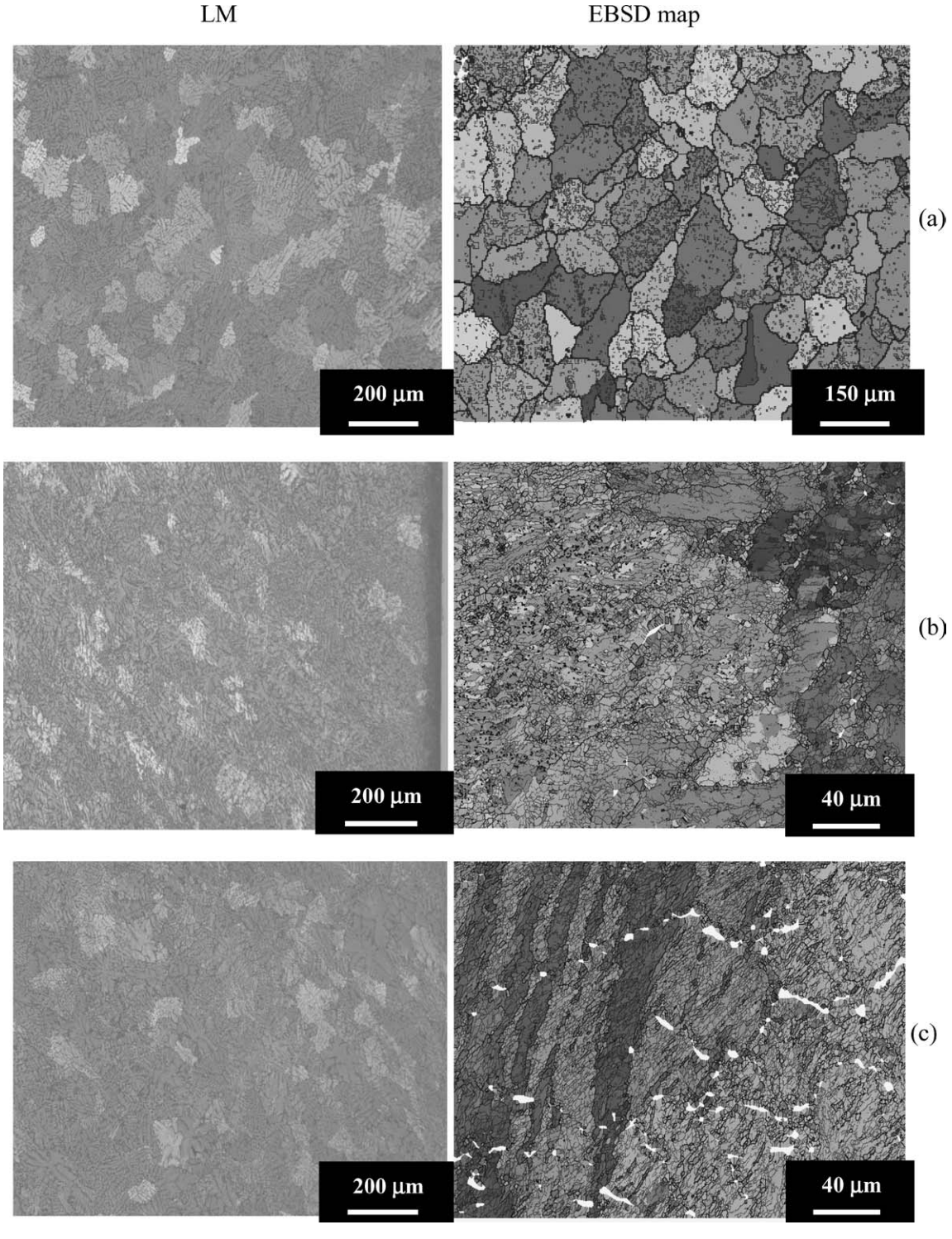

Figure 3 Representative LM micrographs and EBSD maps of the 3103 alloy for the not-deformed (a), after 2 pass (b), and 3 passes (c) conditions In the EBSD maps, the thick black lines stand for grain boundaries.

the Hall Petch (H-P) relationship. The H-P relationship [24, 25] relates yield stress, σ_y to grain size, d, through the Equation 2:

$$\sigma_y = \sigma_0 + k_y d^{-1/2} \tag{2}$$

where σ_0 is the friction stress and k_y is a positive constant of yielding related to the stress required to extend the dislocation activity into adjacent unyielded grains. Since the hardness of a material, HV, as measured using a pyramidal indenter, is proportional to the yield stress expressed by $HV \sim 3\sigma_y$ [25], it follows that Equation 2 can be replaced by Equation 3a:

$$HV = H_0 + kd^{-1/2} \tag{3a}$$

where H_0 and k are appropriate constants associated with hardness data. By estimating the two constants, H_0 and k, for both alloys, it was possible to describe and follow the grain growth induced by the heat treatment. Annealed (at $T = 340^{\circ}$C for 1 to 8 h) and ECA pressed specimens were used to evaluate micro-hardness dependency on grain size. By plotting hardness values as a function of $d^{-1/2}$ and interpolating either the calculated

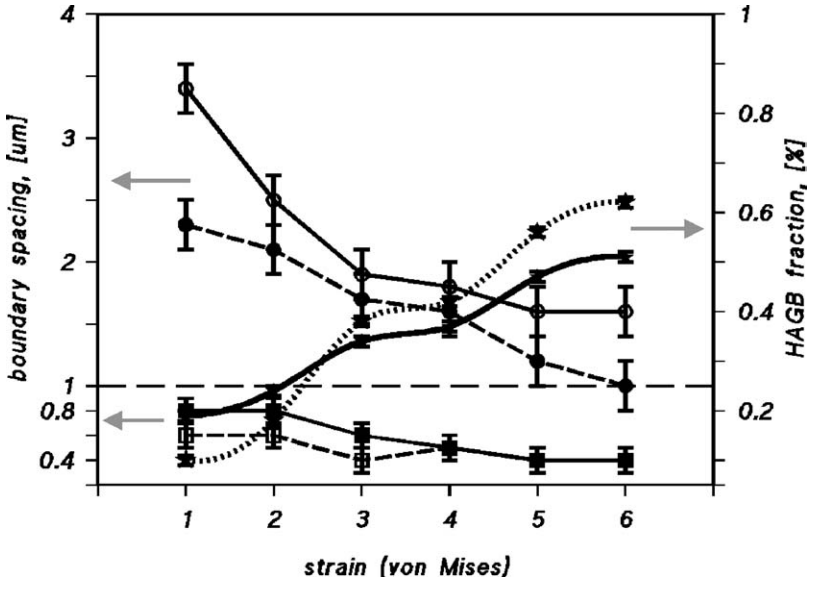

Figure 4 HAGB fraction, grain and subgrain spacing as a function of the true strain (ECAP passes). Circle data points refer to grain spacing, square ones to subgrain spacing, and star ones to the HAGB fraction. Dashed connecting lines refer to 1200 alloy, while solid connecting lines refer to 3103 alloy.

points (generated by micro-hardness and grain size measurements) belonging to the annealed data, and the ones belonging to the ECA pressed data, it was possible to estimate the two constants H_0 and k appearing in Equation 3a:

$$HV_{AA1200} = 35[HV] + 22[HV\mu\mathrm{m}^{1/2}]d^{-1/2} \quad \text{for 1200 alloy} \qquad (3b)$$

$$HV_{AA3103} = 30.9[HV] + 54[HV\mu\mathrm{m}^{1/2}]d^{-1/2} \quad \text{for 3103 alloy} \qquad (3c)$$

Fig. 5a and b report the plots of Equations 3b and 3c, respectively. The H-P relationship was then used to investigate the thermal stability of both alloys subjected to ECAP: micro-hardness tests, were conducted to evaluate grain size using the H-P Equation 3b for the

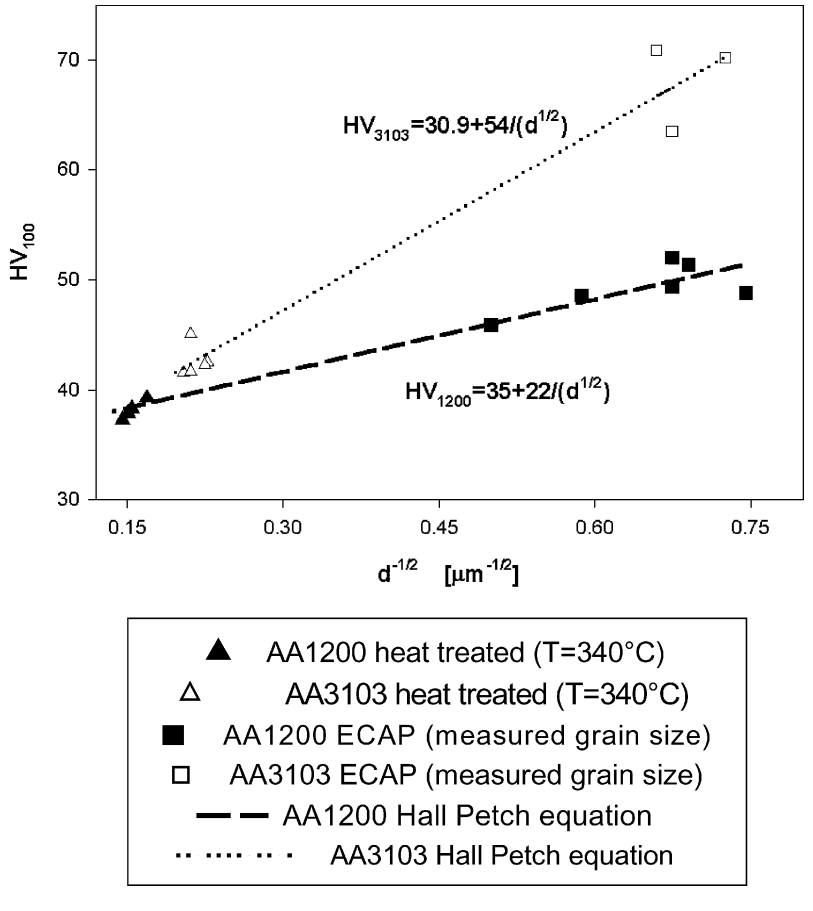

Figure 5 Plot of the Hall-Petch relationship as a function of the number of ECAP passes and following heat treatment ($T = 340^{\circ}$C for 1 to 8 h) for 1200 and 3103 alloys. The plot reports the two interpolating H-P constants, H_0 and k.

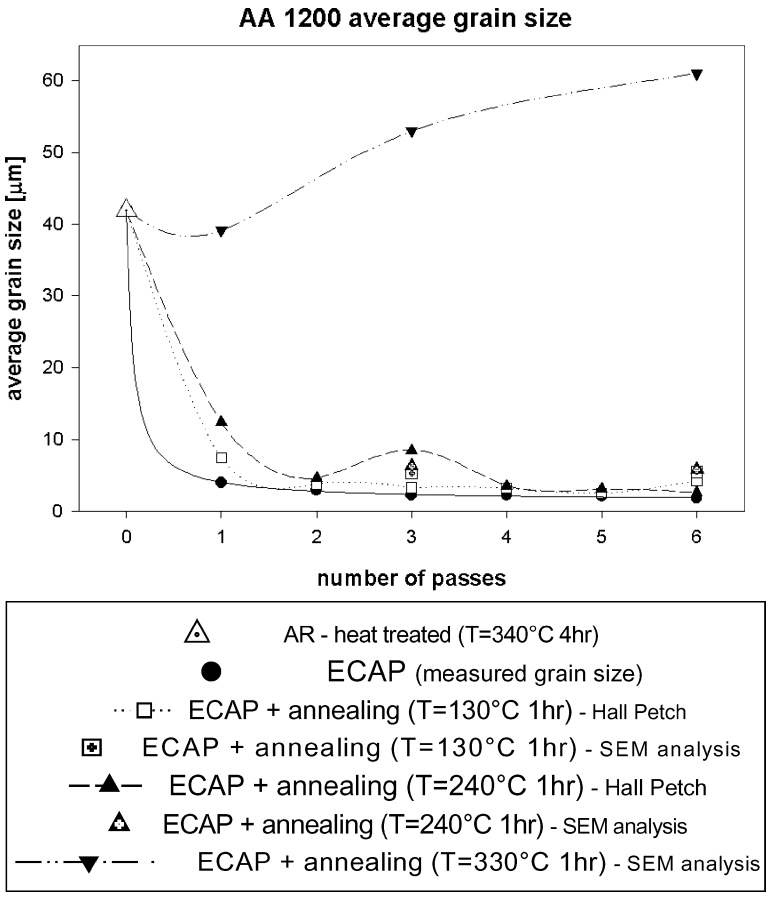

(a)

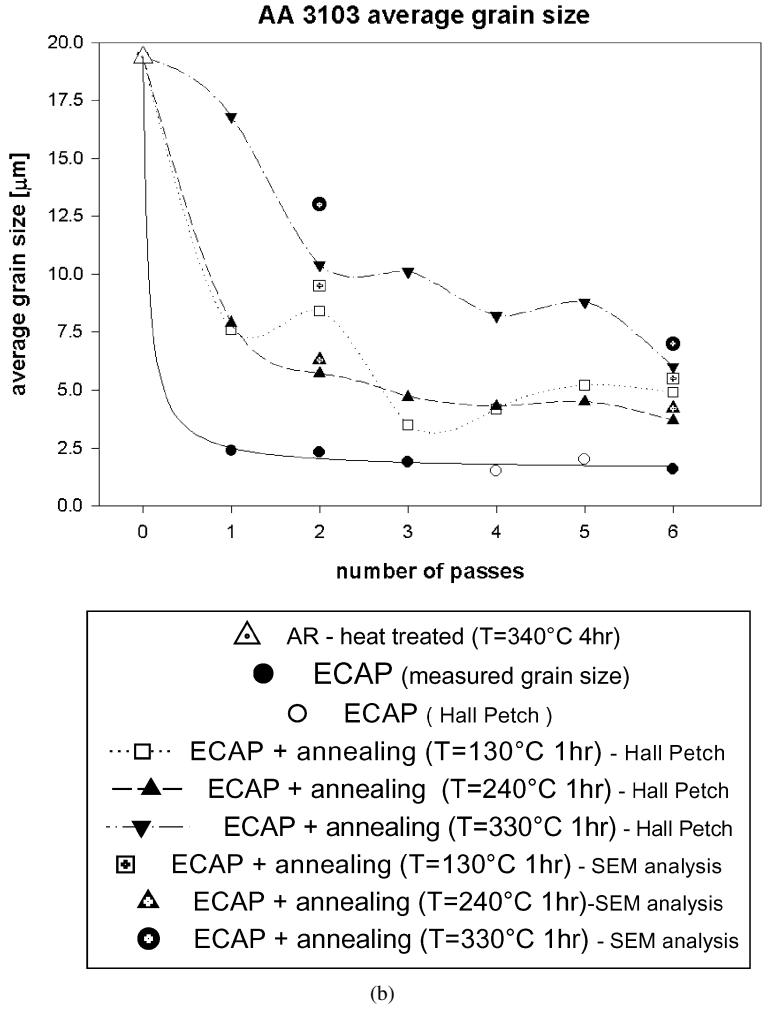

(b)

Figure 6 Grain size as a function of heat treatment and number of ECAP passes: (a) 1200 and (b) 3103 alloy.

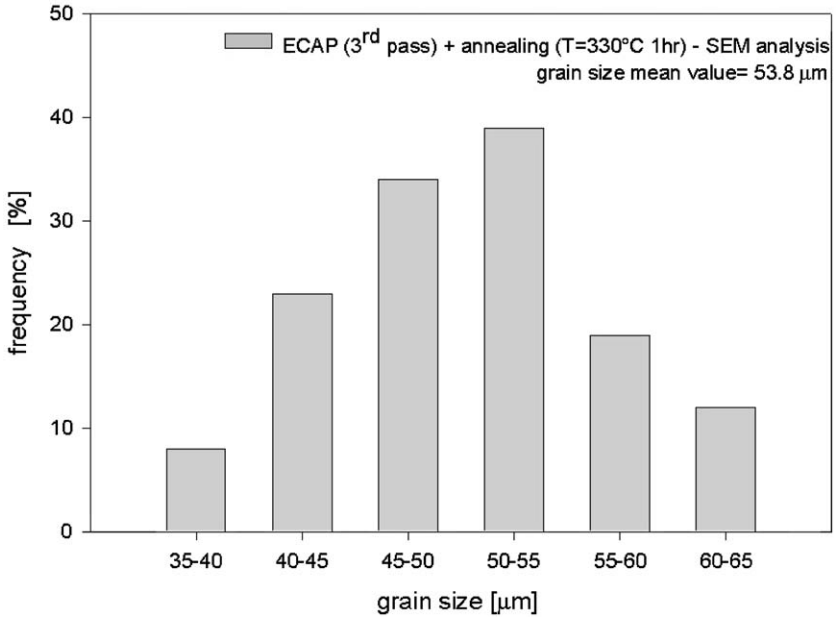

Figure 7 Statistical evaluation and distribution of grain size for the 1200 alloy subjected to 3 ECAP passes and after heat treatment at $T = 330^{\circ}$C/1 h. The reported data were acquired throughout scanning electron microscopy (SEM) inspections.

1200 and the H-P Equation 3c for the 3103 alloy, as a function of the number of ECAP passes and subsequent heat treatment at $T = 130^{\circ}$C ($0.2 \cdot T_m$), 240°C ($0.35 \cdot T_m$), 330°C ($0.5 \cdot T_m$) for 1 h. The results are reported in Fig. 6a and b. Results were validated by SEM investigations of selected specimens (3rd and 6th pass for 1200, 2nd and 6th pass for 3103). They showed good agreement between experimental results and analytical calculations, with the exception of the 1200 alloy subjected to ECAP and subsequent heat treatment at 0.5 T_m. Indeed, the micro-hardness tests showed values close to $H_0 = 35$ HV in Equation 4b; the H-P relationship was thus proved unreliable in such experimental conditions. Moreover, direct SEM evaluation of grain size evidenced consistent differences from 1200 samples subjected to heat treatment at lower temperatures. SEM statistical analysis of grain size for the 1200 alloy subjected to 3 passes (Fig. 7) revealed a mean grain size of 54 μm, which exceeds even the one of the non-deformed material. At this temperature and after 6 ECAP passes, grain growing up to 60 μm (i.e., 50% more than in the non-deformed condition) took place in the 1200 alloy. The grain size increase with ECAP passes followed by high-temperature exposure was attributed to the motion of high-density dislocations, which rearranged to form grain boundaries. This effect was basically attributed to the high dislocation density within the grains present in the microstructure of both materials subjected to a even number of passes. A higher dislocation density was generated by the rising number of passes. Thus, subsequent high-temperature exposure promoted the rearrangement of this forest of dislocations toward the existing grain boundaries. The grain boundaries were induced to move as well. This thermally activated mechanism was responsible for the more effective grain growth that took place with each additional ECAP pass. This way, high-temperature exposure (0.5 T_m for 1 h) was sufficient for a dramatic grain growth capable of reaching mean values far higher than those observed in the as-received 1200 alloy, destroying the beneficial refining effect of the severe plastic deformation imposed through ECAP. Yet, at annealing temperatures of 0.2–0.35 T_m, hardness tests showed quite good agreement with the Hall-Petch relationship, giving grain size in the range 0.5–25 μm. The results reported in Fig. 5a and b imply that the refined microstructure, produced by ECAP, is unstable for temperatures exceeding 0.35 T_m. It is well known that superplasticity requires temperatures in the order of at least 0.5 T_m (~330°C for both 1200 and 3103); thus, the ECA pressed microstructure is unstable in the temperature range associated with the high super-plastic ductility. This basic result suggests that the ECAP-induced microstructural evolution taking place in aluminum-based alloys containing fine dispersoids or precipitates (responsible for the inhibition of grain growth under annealing treatments) should be investigated using FEG-SEM EBSD, together with TEM inspections. A limited fraction of less than 0.15% of Zr, Sc or Ti is able to produce a microstructure decorated with very fine Zr-, Sc- or Ti-bearing dispersoids capable of pinning grain boundary movement by exposing the material to high temperatures.

5. Conclusions

Two aluminum alloys, 1200 and 3103, were ECA pressed to six passes using the "route" C. The severe plastic deformation induced the formation of a microstructure decorated by grain size mostly of $1 \div 2$ μm after six passes for either material. Grain and subgrain spacing and their misorientation distribution were evaluated by means of EBSD techniques in a FEG-SEM, and the grained microstructure stability was detected. The results can be summarized as follows:

- Misorientation increased at each ECAP pass, and increasing subgrains misorientation allowed them

to transform into fine grains already after 3 passes in both alloys. In particular, the refinement process was more effective in the 3103 alloy.

- HAGB fraction continuously increased with the strain at the expense of the subgrains formed during the SPD.
- Thermal stability studies were carried out for temperatures ranging 130–330°C, corresponding to 0.2–0.5 of the alloys melting temperature. For both alloys, the fine grain structure was stable at temperatures under 240°C (0.35 T_m); whereas, in the range of super-plasticity temperatures, a consistent grain growth occurred and the refining effect of ECA pressing was completely lost. This way, the fine microstructure induced by ECAP was not stable at temperatures in the range of superplasticity. Microstructure refinement, induced by ECA pressing 1200 and 3103 aluminum-based alloys, may be stabilized by adding fine dispersoids or precipitates (responsible for the inhibition of grain growth under annealing treatments). As a matter of facts, a limited fraction of less than 0.15% of Zr, Sc or Ti is able to produce a microstructure decorated by very fine Zr-, Sc- or Ti-bearing dispersoids capable of pinning grain boundary movement by exposing the material to high temperatures.

Acknowledgements

The work was supported by research funds from the INFM PAIS-UFIGRAL project. The authors are grateful to Mr. D. Ciccarelli and Mr. M. Pieralisi for their assistance in the LM specimen preparation.

References

1. R. Z. VALIEV, R. K. ISLAMGALIEV and I. V. ALEXANDROV, *Prog. Mater. Sci.* **45** (2000) 103.
2. V. M. SEGAL, V. I. REXENIKOV, A. E. DOBYSHEVSKIJ and V. I. KOPYLOV, *Metally* **1** (1982) 115 (translation from: Russian Metallurgy **1** (1981) 99).
3. A. GHOLINA, P. B. PRANGNELL and M. V. MARKUSHEV, *Acta Mater.* **48** (2000) 1115.
4. J. R. BOWEN, O. V. MISHIN, P. B. PRANGNELL and D. JUUL JENSEN, *Scripta Mater.* **47** (2002) 289.
5. A. GHOLINA, P. BATE and P. B. PRANGNELL, *Acta Mater.* **50** (2002) 2121.
6. A. GHOLINA, J. R. BOWEN, P. B. PRANGNELL and F. J. HUMPHREYS, in Proceedings of the 6th Int. Conf. on Al-Alloys ICAA-6, edited by T. Sato, S. Kumai, T. Kobayashi and Y.T. Murakami (The Japan Institute of Light Metals, Tokyo, 1998) Vol. 1, p. 577.
7. P. B. BERTON, N. K. TSENEV, R. Z. VALIEV, M. FURUKAWA, Z. HORITA, M. NEMOTO and T. G. LANGDON, *Metall. Mater. Trans.* A **29** (1998) 2237.
8. B. BAY and N. HANSEN, in Proceedings of the Risø Int. Conf. on Annealing Process: Recovery, Recrystallization and Grain Growth 1986, edited by N. Hansen, D. Juul Jensen, T. Leffers and B. Ralph, p. 215.
9. Y. IWAHASHI, Z. HORITA, M. NEMOTO and T. G. LANGDON, *Acta Mater.* **46** (1998) 3317.
10. J. Y. CHANG, J. S. YOON and G. H. KIM, *Scripta Mater.* **45** (2001) 347.
11. G. PALOMBO, U. ERB and K. T. AUST, *ibid.* **24** (1990) 2347.
12. C. SURYANARAYANA, D. MUKHOPADHYAY, S. N. PANTANKAR and F. H. FROES, *J. Mater. Res.* **7** (1992) 2114.
13. Z. HORITA, T. FUJINAMI, M. NEMOTO and T. G. LANGDON, *J. Mater. Proc. Techn.* **117** (2001) 288.
14. O. A. KAIBISHEV, *ibid.* **117** (2001) 300.
15. Z. HORITA, T. FUJINAMI, M. NEMOTO and T. G. LANGDON, *Metall. Mater. Trans.* A **31** (2000) 691.
16. M. FURUKAWA, Y. IWAHASHI, Z. HORITA, M. NEMOTO and T. G. LANGDON, *Mater. Sci. Eng.* A **257** (1998) 328.
17. K. NAKASHIMA, Z. HORITA, M. NEMOTO and T. G. LANGDON, *Acta Mater.* **46** (1998) 1589.
18. Y. IWAHASHI, J. WANG, Z. HORITA, M. NEMOTO and T. G. LANGDON, *Scripta Mater.* **35** (1996) 143.
19. P. L. SUN, P. W. KAO and C. P. CHANG, *Mater. Sci. Eng.* A **283** (2000) 82.
20. A. SHAN, I. G. MOON and J. W. PARK, *J. Mater. Proc. Techn.* **122** (2002) 255.
21. E. NES, A. L. DONS and N. RYUM, in Proceedings of ICSMA 6, 1982, edited by R. C. Gifkins (Pergamon Press, 1982) p. 425.
22. S. D. TERHUNE, D. L. SWISHER, K. OH-ISHI, Z. HORITA, T. G. LANGDON and T. R. McNELLEY, *Metall. Mater. Trans.* A **33A** (2002) 2173.
23. P. J. HURLEY, P. S. BATE and F. J. HUMPHREYS, *Acta Mater.* **51** (2003) 4737.
24. R. CROOKS S. J. HALES and T. R. McNELLEY, in Proceedings of Int. Conf. on Superplasticity and Superplastic Forming 1998, edited by C. H. Hamilton and N. E. Paton (The Minerals, Metals and Materials Society) p. 389.
25. M. FURUKAWA, Z. HORITA, M. NEMOTO, R. Z. VALIEV and T. G. LANGDON, *Acta Mater.* **44** (1996) 4619.

Received 1 December 2003
and accepted 30 April 2004